Effective Date: 12·19·07

WP 08-PT.15

Revision 0

Regulatory Hypothetical Accident Condition Type B Testing for the HalfPACT Shielded Container Payload

Cognizant Department: Packaging

Approved by: Ria Barnett for T.E. Sellmer

TABLE OF CONTENTS

1.0 Introduction 1
2.0 References 1
3.0 Testing Responsibilities 1
4.0 Test Article Description 2
4.1 Shielded Containers 2
4.2 Simulated Payload 2
4.3 Payload Support Components 4
4.4 HalfPACT Inner Containment Vessel (ICV) 6
5.0 Technical Basis for the Tests 8
5.1 Justification for Testing Only End and Side Orientations 8
5.1.1 End Drop 9
5.1.2 Side Drop 10
5.2 Temperature 12
5.2.1 Cold 12
5.2.2 Hot 14
5.3 Pressure 15
6.0 Test Results 16
6.1 Component Weights 16
6.2 Free Drop Tests 16
6.2.1 Vertical End Drop Preparation and Test 19
6.2.2 Post-End Drop Test Disassembly 19
6.2.3 Horizontal Side Drop Test Preparation and Test 25
6.2.4 Post-Side Drop Test Disassembly 25
6.3 Shielding Integrity Testing 33

LIST OF FIGURES

Figure 1 – Shielded Container Configuration 3
Figure 2 – 30-Gallon Drum with a Simulated Payload 4
Figure 3 – Exploded View of the Payload Assembly 5
Figure 4 – Sectioned View of the Payload Assembly 6
Figure 5 – Plastic Stretch-Wrapped Shielded Containers 7
Figure 6 – Bottom Reinforcement for the HalfPACT ICV 7
Figure 7 – Test Configuration and Orientations 11
Figure 8 – Installing and Cutting the Fluorescein Dye Bags 17
Figure 9 – Wetting the Container to Activate the Fluorescein Dye 17
Figure 10 – Fluorescein Dye within the Shielded Container Body 18

Figure 11 – Fluorescein Dye under the Shielded Container Lid 18
Figure 12 – 30-foot End Drop.....20
Figure 13 – Instant of End Drop Impact 20
Figure 14 – End Drop Hoop Damage to the ICV Shell (Overall) 21
Figure 15 – End Drop Hoop Damage to the ICV Shell (Close-Up) 21
Figure 16 – Pre-End Drop Relative Position of Components.....22
Figure 17 – Post-End Drop Relative Position of Components 22
Figure 18 – Deformed Pallet, Axial Dunnage, and Lower Spacer 23
Figure 19 – Deformed Lower Axial Dunnage from End Drop.....23
Figure 20 – Deformed Lower Spacer (from End Drop; Top View) 24
Figure 21 – Deformed Lower Spacer (from End Drop; Bottom View).....24
Figure 22 – Temporary Lower Spacer Structure Used for Side Drop 27
Figure 23 – Pre-Side Drop Test Shield Container Configuration.....27
Figure 24 – Side Drop Impact Orientation (2º Off True Horizontal) 28
Figure 25 – 30-foot Side Drop 28
Figure 26 – Instant of Side Drop Impact/Rebound.....29
Figure 27 – Deformed ICV Lid (~26” Flat) after Side Drop 29
Figure 28 – Lateral Shifting of the Payload after Side Drop 30
Figure 29 – Dimensions Relating the Shifted Shielded Containers.....30
Figure 30 – Side Drop Deformed Radial Dunnage (Outside View).....31
Figure 31 – Side Drop Deformed Radial Dunnage (Inside View).....31
Figure 32 – Negligible Visible End or Side Drop Damage 32
Figure 33 – Side Drop Damage Limited to Localized Weld Crushing.....32
Figure 34 – Scanning Apparatus.....33
Figure 35 – Circumferential and Axial Scan Grid Map.....34
Figure 36 – Shielding Change on Test Shielded Container B01 35
Figure 37 – Shielding Change on Test Shielded Container B02 36
Figure 38 – Shielding Change on Test Shielded Container B03 37
Figure 39 – Axial Slice in B03 at Lowest Point; Lower End 39
Figure 40 – Axial Slice in B03 at Lowest Point; Upper End.....39
Figure 41 – Axial Slice in B03 at B02 Interface; Lower End.....40
Figure 42 – Axial Slice in B03 at B02 Interface; Upper End 40

LIST OF TABLES

Table 1 – Component Weights (lb).....16
Table 2 – Measured Lead Thickness (Inches) in Test Unit B03 Axial Slices 41

1.0 INTRODUCTION

Three shielded containers containing specific transuranic waste forms are planned to be transported within each HalfPACT package. This report documents 30-foot free drop tests per the regulatory Hypothetical Accident Conditions (HAC) described in 10 CFR §71.73 [1] to support the licensing activities for the shielded container payload configuration.

Three shielded containers were assembled on a triangular spaceframe pallet and installed, including axial and radial dunnage assemblies, within a HalfPACT inner containment vessel (ICV). The package was subjected to two 30-foot free drops onto a flat, essentially unyielding, horizontal surface. The package was dropped such that the package impacted the target surface in a position to maximize shielded container damage. The HalfPACT outer containment assembly (OCA), with its energy absorbing polyurethane foam, was conservatively omitted from the tests. At the conclusion of the second 30-foot free drop, each shielded container was removed from the ICV and subjected to shielding integrity testing to verify shielding integrity and visually scanned for the presence of fluorescein dye to verify confinement integrity.

All tests were documented via video and still photography to provide a visual record of events.

2.0 REFERENCES

1. Title 10, Code of Federal Regulations, Part 71 (10 CFR 71), *Packaging and Transportation of Radioactive Material*, 01-01-07 Edition.

2. ES-A-001, *Engineering Specification for Drop Test Pad for Type A Performance Testing*, Revision 0, Westinghouse Engineered Products Department, 1998.

3. U.S. Department of Energy (DOE), *Safety Analysis Report for the HalfPACT Shipping Package*, USNRC Certificate of Compliance 71-9279, U.S. Department of Energy, Carlsbad Field Office, Carlsbad, New Mexico.

4. U.S. Department of Energy (DOE), *Safety Analysis Report for the TRUPACT-II Shipping Package*, USNRC Certificate of Compliance 71-9218, U.S. Department of Energy, Carlsbad Field Office, Carlsbad, New Mexico.

5. U.S. Department of Energy (DOE), *Safety Analysis Report for the RH-TRU 72-B Waste Shipping Package*, USNRC Certificate of Compliance 71-9212, U.S. Department of Energy, Carlsbad Field Office, Carlsbad, New Mexico.

6. MIL-HDBK-5J, *Metallic Materials and Elements for Aerospace Vehicle Structures*, Department of Defense Handbook, 31 January 2003.

3.0 TESTING RESPONSIBILITIES

Washington TRU Solutions (WTS) was responsible for the overall test program, including directing testing activities, as follows:

- Approving the shielded container, pallet, and dunnage drawings and detailed test procedures,
- Providing a TRUPACT-II ICV, with aluminum honeycomb end spacers, to Engineered Products Department for modification to reflect the configuration of a HalfPACT ICV,

- Providing engineering support during fabrication,
- Providing engineering oversight during the testing process, and
- Preparing this test report.

Engineered Products Department (EPD) was responsible for fabricating and testing the shielded container configuration, as follows:

- Preparing a test procedure that included test preparation, pre- and post-drop shield integrity tests of each shielded container, free drop test details, and post-drop test documentation,
- Fabricating three shielded containers (see Section 4.1, *Shielded Containers*), three payloads (see Section 4.2, *Simulated Payload*,) and payload support components (see Section 4.3, *Payload Support Components*), in accordance with approved drawings and procurement documentation,
- Modifying a TRUPACT-II ICV to shorten it to a HalfPACT ICV configuration, stiffening the ICV bottom, and installing test lifting and handling attachments,
- Providing facility personnel and equipment, including photometrics, for the testing process; the drop test pad is documented in ES-A-001 [2],
- Performing drop testing, pre- and post-test shielding integrity testing, and disassembly as, directed by WTS,
- Providing 10 CFR 71, Subpart H, QA oversight during fabrication, test procedure development, testing, pre- and post-test shielding integrity testing, and dimensional inspections, and
- Providing the necessary measuring and test equipment (M&TE) for documenting fabrication, testing, and pre- and post-test measurements.

4.0 TEST ARTICLE DESCRIPTION

4.1 Shielded Containers

The shielded container is a 23-inch diameter, 35¾-inch tall cylindrical vessel with nominally 1-inch of lead shielding inside of 7-gauge inside and 11-gauge outside steel body shells and 3 inches of steel shielding in the lid and base, weighing approximately 1,726 pounds empty. It is designed to carry a 30-gallon payload drum with a special top lever-lock closure, where the loaded payload container has a maximum gross weight limit of 2,260 pounds. The shielded container also includes a filter port through the lid, and a silicone rubber gasket between the lid and the body. Figure 1 illustrates the shielded container.

4.2 Simulated Payload

The 30-gallon drums were fitted with a slotted 8-inch diameter, 27-inch long Sonotube® filled with concrete, as shown in Figure 2. A 1/2-inch diameter rebar embedment was used as a provision for handling the loaded 30-gallon drum.

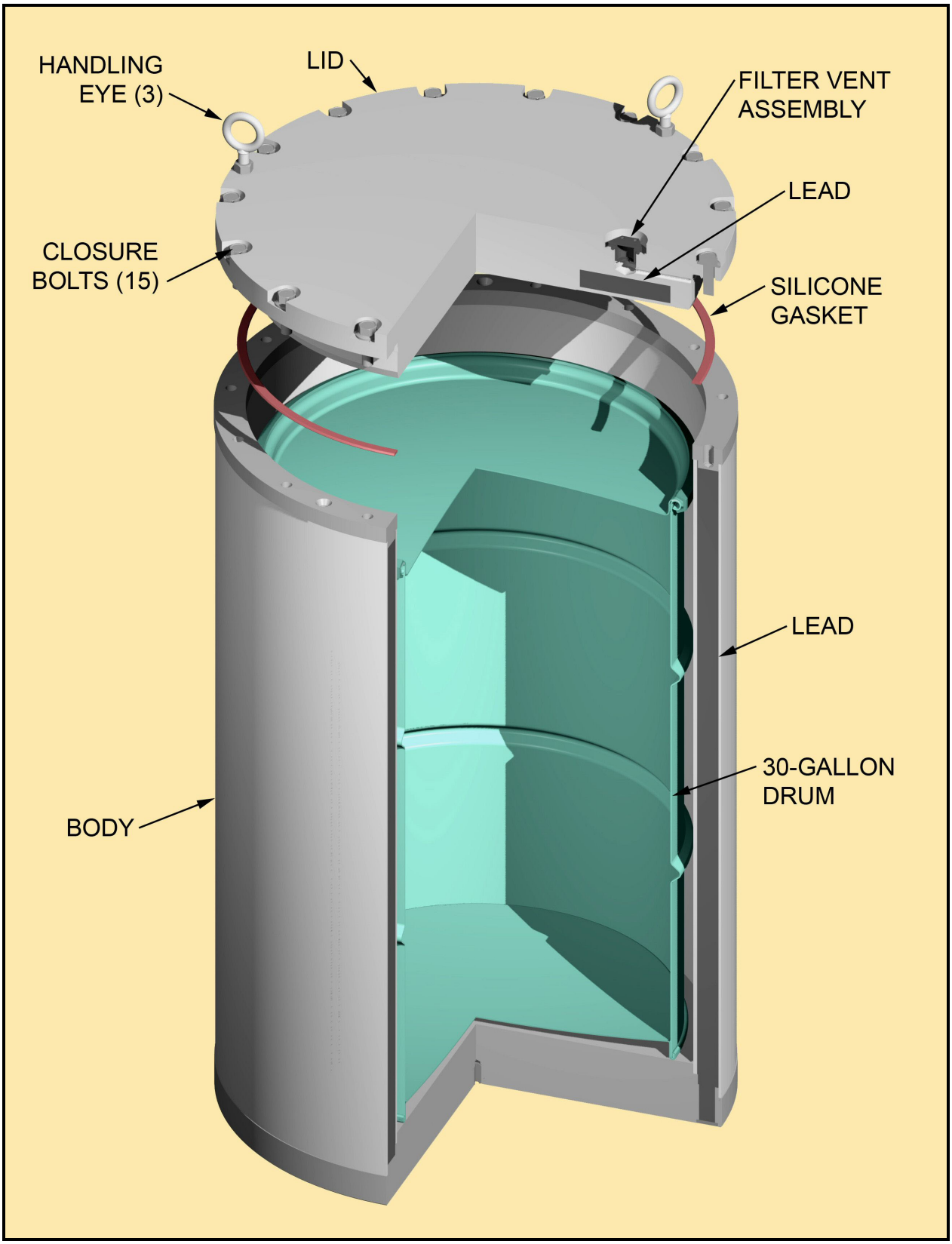

Figure 1 – Shielded Container Configuration

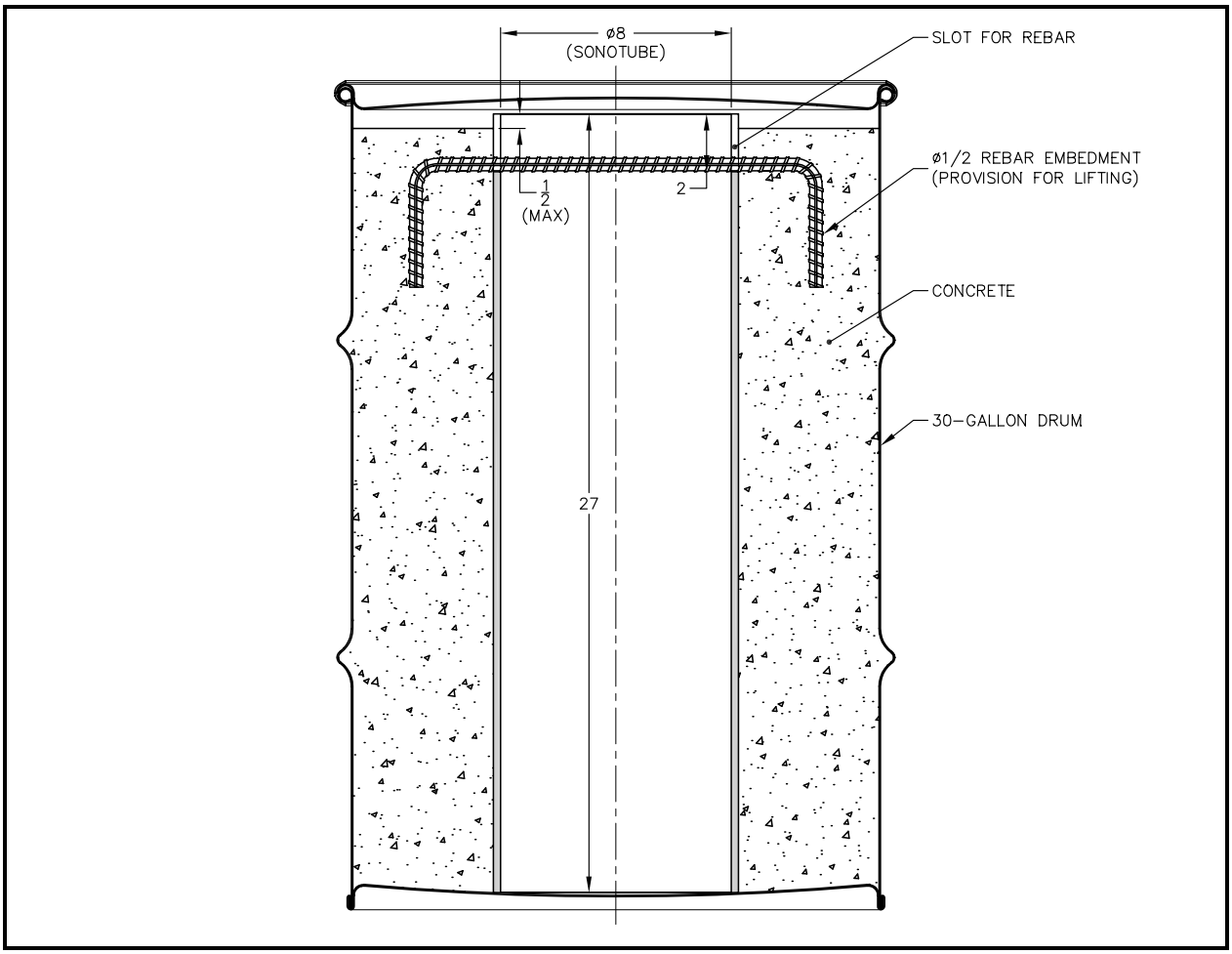

Figure 2 – 30-Gallon Drum with a Simulated Payload

Based on the actual measured weights of the three, as-built shielded containers and payload support components, the gross weight of each test payload, with lid and lever lock closure, was set at 560 pounds. Sand was added to the inside of the Sonotube® to achieve the desired weight. Using 560-pound, 30-gallon payload containers was conservative for addressing the shielded containers and ensured that a) the total weight of each shielded container exceeded its 2,260-pound maximum gross weight and b) the total weight of all payload components was equal to the maximum HalfPACT payload capacity of 7,600 pounds (see Table 1).

4.3 Payload Support Components

As shown in Figure 3 and Figure 4, the payload support components consist of radial dunnage, axial dunnage at the top and bottom, a bottom slipsheet, a top reinforcing plate, and a triangular spaceframe pallet. The top reinforcing plate and bottom slipsheet were omitted for testing. The three shielded containers were plastic stretch-wrapped after positioning on the triangular spaceframe pallet (see Figure 5).

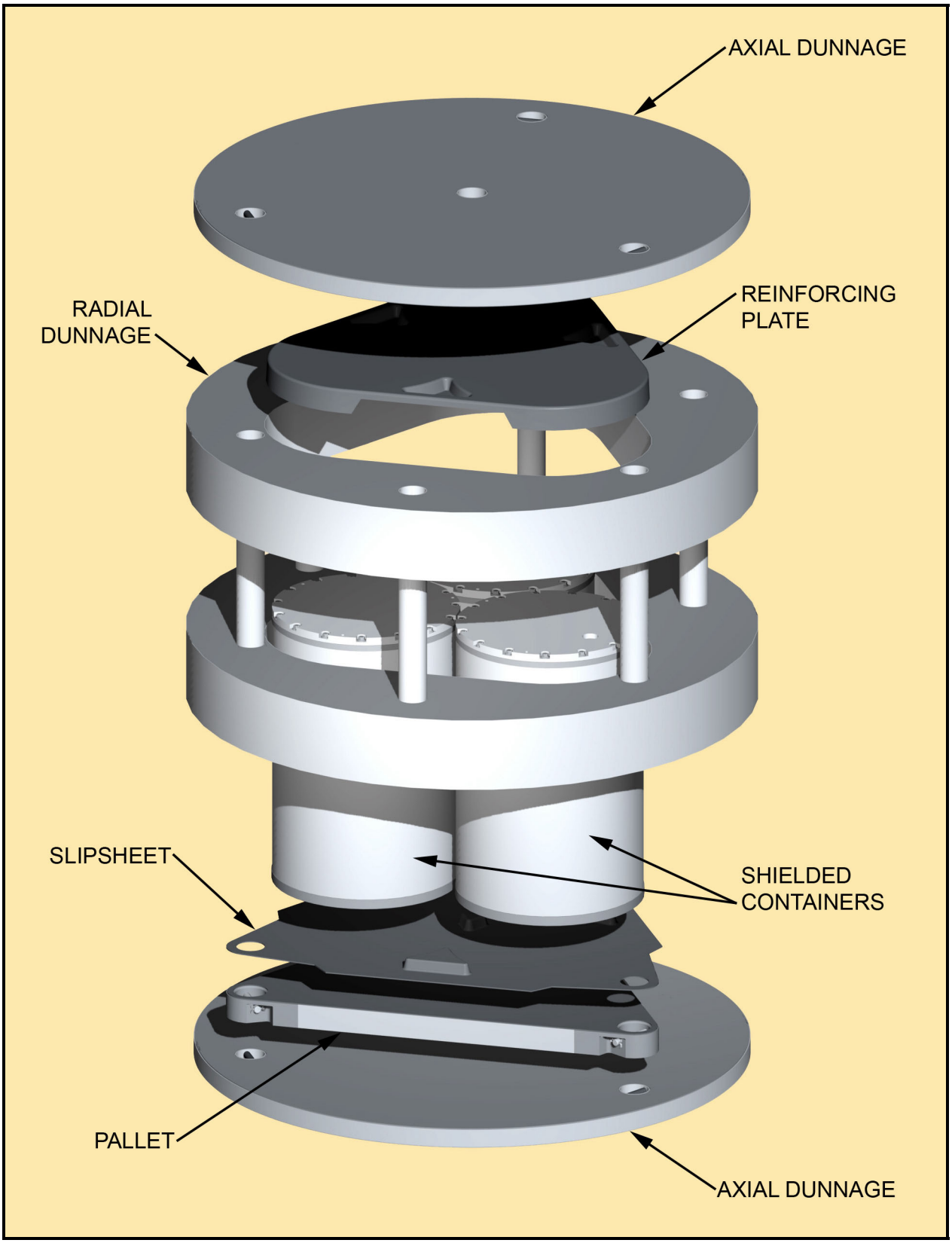

Figure 3 – Exploded View of the Payload Assembly

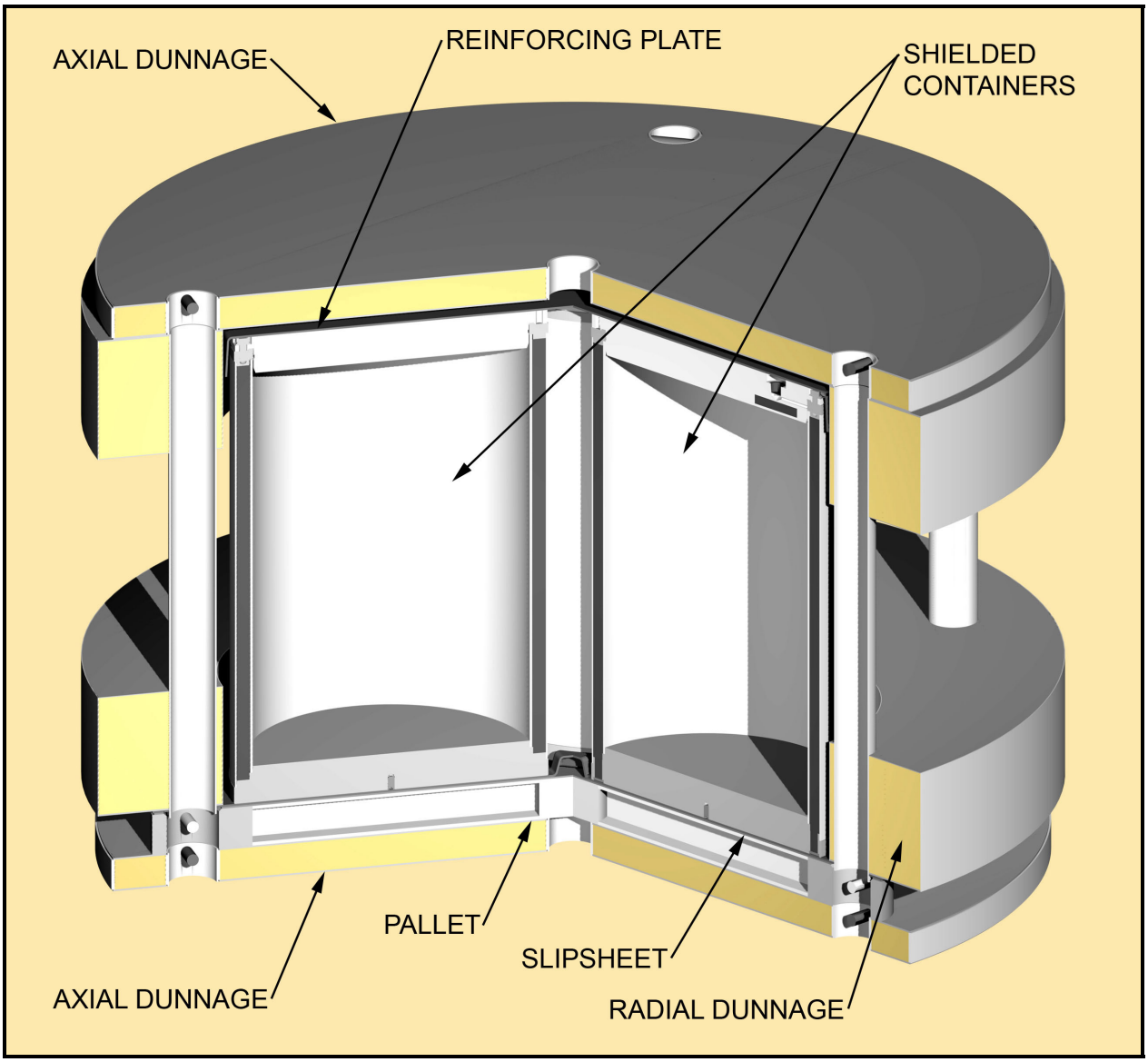

Figure 4 – Sectioned View of the Payload Assembly

4.4 HalfPACT Inner Containment Vessel (ICV)

Testing utilized a prototypic HalfPACT ICV, cut down from a TRUPACT-II ICV, but without a locking ring. The lid was attached to the body via welding. Both the upper and lower aluminum honeycomb spacers were used.

Eight radial stiffeners and a single circumferential ring stiffener were added to stiffen the ICV bottom for the bottom end drop (see Figure 6). The quantity of stiffeners was designed to produce impact forces equal to or greater than the maximum measured during TRUPACT-II testing (see Section 5.1.1, *End Drop*, for a relevant discussion).

Lifting attachments and appropriate rigging hardware were installed as necessary to allow handling and control of orientation of the ICV for each drop test.

Figure 5 – Plastic Stretch-Wrapped Shielded Containers

Figure 6 – Bottom Reinforcement for the HalfPACT ICV

5.0 TECHNICAL BASIS FOR THE TESTS

The following subsections supply the technical basis for the chosen free drop test orientations and initial conditions (temperature and pressure). As shown, performance capabilities are adequately demonstrated by ambient temperature, free drop testing of the bottom end and side drop orientations. Other drop test orientations are shown to have less significance than end and side, and observed ambient temperature performance was such that conservative analytic extrapolations to temperature extremes (hot and cold) coupled with the inherent strength of the relatively robust shielded container design readily demonstrate acceptable performance at those extremes.

Key test observations (see Section 6.0, *Test Results*) that support the conclusions presented herein and allow for use of conservative analytic extrapolations to temperature extremes are as follows:

1. The three shielded containers were conservatively subjected to cumulative drop damage (both end and side) rather than using previously undamaged/dropped units for each test.

2. Post-test visual inspection of the interior and exterior surfaces of the three shielded containers indicated no apparent global or localized deformation or damage to the shielded containers. The solid, concrete-filled rolling hoops in the 30-gallon test payload drums left no visible deformation of the shielded container's inner shell, even through these drums were loaded to exceed the 2,260-pound shielded container gross weight (see Table 1). Visible damage was limited to localized flattening (~2 inches long) of the outer shell-to-flange/base welds in contact at shielded container to shielded container interfaces during the side drop event.

3. Post-test visual inspection of the HalfPACT ICV shell at its interface with payload dunnage components revealed no localized deformations that could in any way compromise containment integrity.

4. Subsequent to the performance of end and side drop testing, most closure bolts retained full residual torque, and all closure bolts retained some residual torque; 4 bolts on test shielded container B01, no bolts on test shielded container B02, and 1 bolt on test shielded container B03 lost a portion of their torque. In addition, the flour/fluorescein mixture placed within each shielded container was 100% retained throughout the testing. Collectively, these observations readily confirmed confinement integrity of the shielded containers.

5. Pre- and post-test shielding integrity tests coupled with destructive disassemblies of selected shielded container side walls showed no evidence of lead slump or changes of any significance to the shielding capabilities of the design. Post-test visual inspection of the shielded container wall cut-outs revealed some modest global and localized shell deformation, but the magnitudes were very limited, of no structural significance, and not coupled with measurable lead thinning or reduction in shielding.

5.1 Justification for Testing Only End and Side Orientations

To address shielded container performance and any potential for adverse effects on the HalfPACT packaging containment boundaries when transporting shielded containers, it is only necessary to perform 30-foot free drop tests for the flat bottom and side orientations. This is because both the radial dunnage assembly and the axial dunnage assemblies (acting in conjunction with the adjacent aluminum honeycomb end spacers) have been independently designed to absorb 100% of the payload energy associated with a 30-foot drop.

In an end drop orientation, virtually all payload-related energy is absorbed by a combination of crushing the aluminum honeycomb end spacer (primary energy absorber) and an axial dunnage assembly (secondary energy absorber). As demonstrated by the bottom end drop testing, the payload pallet structure was minimally deformed and can therefore be assigned no significant energy absorbing role. The radial dunnage assembly also plays no role in an end drop and remains undamaged. Figure 18 through Figure 21 illustrate end drop damage to these components.

Conversely, in a side drop, the payload pallet, axial dunnage, and aluminum honeycomb end spacer assemblies play no role and remain virtually undamaged, while the radial dunnage assembly absorbs all the kinetic energy associated with the three loaded shielded containers (see Figure 30 and Figure 31).

Any drop orientation other than end or side would partially crush both axial and radial energy absorbing dunnage components, but each to a lesser degree than what occurs for the more limiting end and side drop tests. As such, for other drop orientations, loads on both the HalfPACT ICV as well as on the shielded containers themselves would be more distributed (i.e., partially shared by both end and side structures) and of lesser magnitude than those experienced in flat end or side drops. Also, from a post-accident shielding point of view, the greatest shift of the shielded containers within the ICV will occur for the end and side drop tests. Finally, the relatively large post-drop residual radial and axial clearances that existed between the shielded containers and the ICV clearly demonstrated that there is no potential for the shielded containers to directly impact, or in any way compromise, the HalfPACT ICV.

The test configuration and drop orientations are illustrated in Figure 7. As shown, the testing conservatively ignores the presence of the impact attenuating OCA and tests in a bare ICV.

5.1.1 End Drop

The end drop is performed using an unprotected HalfPACT ICV that is conservatively stiffened at its lower end (see Figure 6). Stiffening of the lower head results in a higher overall system deceleration than if testing had instead included the impact attenuating HalfPACT OCA. Per Section 2.10.3.5.2.2 of the HalfPACT SAR [3] for the bottom end drop scenario, the cold impact deceleration acting on the HalfPACT packaging would be 409*g* if the OCA were present. The corresponding ICV shell compressive stress, per that same section, is a relatively modest 12,305 psi. With reference to Figure 14 and Figure 15, given the circumferentially uniform and permanent deformation that occurred just above the stiffeners at the lower end of the ICV shell in the shielded container end drop test (absent in all prior TRUPACT-II and HalfPACT testing that included an OCA), it is clear that stiffening of the ICV for the shielded container testing conservatively bounded the overall system deceleration.

The response of the shielded containers themselves is therefore dictated by the behavior of the lower aluminum honeycomb end spacer and, to a lesser extent, the adjacent axial dunnage assembly. Of note, given the slightly thicker upper aluminum honeycomb end spacer and the dished nature of the upper OCA exterior head versus the flat bottom head (and hence an overall system deceleration for top end drop that is well less than for the bottom end drop), the shielded containers will experience greater loads in a bottom down rather than a top down impact. Nevertheless, for end drop test purposes, one shielded container was inverted with its lid end pointing downward to conservatively simulate the effects of a top end drop on a shielded container.

From the ambient temperature (77 ºF) end drop testing, the shielded containers were observed to stroke approximately 6.2 inches relative to the lower head of the ICV. This deformation can be further broken

down into an approximate 1.25-inch crush of the axial dunnage assembly and 4.95-inch crush for the aluminum honeycomb spacer. However, since the aluminum honeycomb crushes at an essentially constant value and the foam within the axial dunnage will strain harden only up to the point where the applied force on the axial dunnage assembly matches the load carrying capability of the underlying honeycomb, the constant force resistance of the honeycomb can be reasonably assumed to exist for the full 6.2-inch stroke. With the available kinetic energy, E, from the various payload components having a combined weight, W = 7,600 pounds, falling from a height, h = 360 inches, a nominal crush strength, σ_{cr} = 120 psi, for the aluminum honeycomb material (see Table 2.3-3 in the HalfPACT SAR [3]), and the observed end drop stroke, δ = 6.2 inches, the effective crush diameter, d_{eff}, is determined as follows:

$$E = W(h+\delta) = V_{cr}\sigma_{cr} = \left(\frac{\pi}{4}\right)d_{eff}^2\delta\sigma_{cr}$$

Thus,

$$d_{eff} = \sqrt{\frac{4W(h+\delta)}{\pi\delta\sigma_{cr}}} = \sqrt{\frac{4(7{,}600)(360+6.2)}{\pi(6.2)(120)}} = 69.01\,\text{in}$$

Note that this effective diameter makes reasonable physical sense as it is approximately equal to the 68-inch diameter of the axial dunnage assembly. Further, visual inspection of the as-crushed aluminum honeycomb spacer also reasonably confirms the calculated 69.01-inch diameter (see Figure 21).

In summary, with a crush strength of 120 psi and an effective crush diameter of 69.01 inches for the aluminum honeycomb end spacer, the crush force becomes 448,844 pounds, or equivalently, 59.1*g* acting on the 7,600 pounds of payload components in the ambient temperature end drop test. Impact accelerations at temperature extremes will be proportional to the strength of the aluminum at those temperature extremes, with the force that is able to develop in the axial dunnage assembly again being limited to the force that can be supported by the honeycomb end spacer itself. As such, the temperature sensitivity of the foam used in the axial dunnage assemblies is of no significance when it comes to establishing end drop impact magnitudes.

5.1.2 Side Drop

The side drop is also conservatively performed using an unprotected HalfPACT ICV (i.e., without the energy absorbing HalfPACT OCA). The aluminum honeycomb end spacer, axial dunnage, and pallet assemblies at the ends of the shielded containers remain undamaged in a side drop, but serve to maintain the relative position of the containers within the radial dunnage assembly and ICV. For this reason, the lower honeycomb end spacer and axial dunnage assembly that were damaged in the end drop test were removed and replaced prior to the side drop test with a steel space frame of the correct overall height to re-center the shielded containers within the ICV and radial dunnage assembly (see Figure 22).

In the case of a side drop, the radial dunnage assembly must absorb all of the drop induced kinetic energy of the shielded containers. To maximize damage to the radial dunnage assembly and maximize the load acting on a single shielded container for the side drop test, the shielded containers were oriented as shown in the top view of Figure 7. This orientation places both a single shielded container and the least amount of radial dunnage thickness directly in line with the impact point.

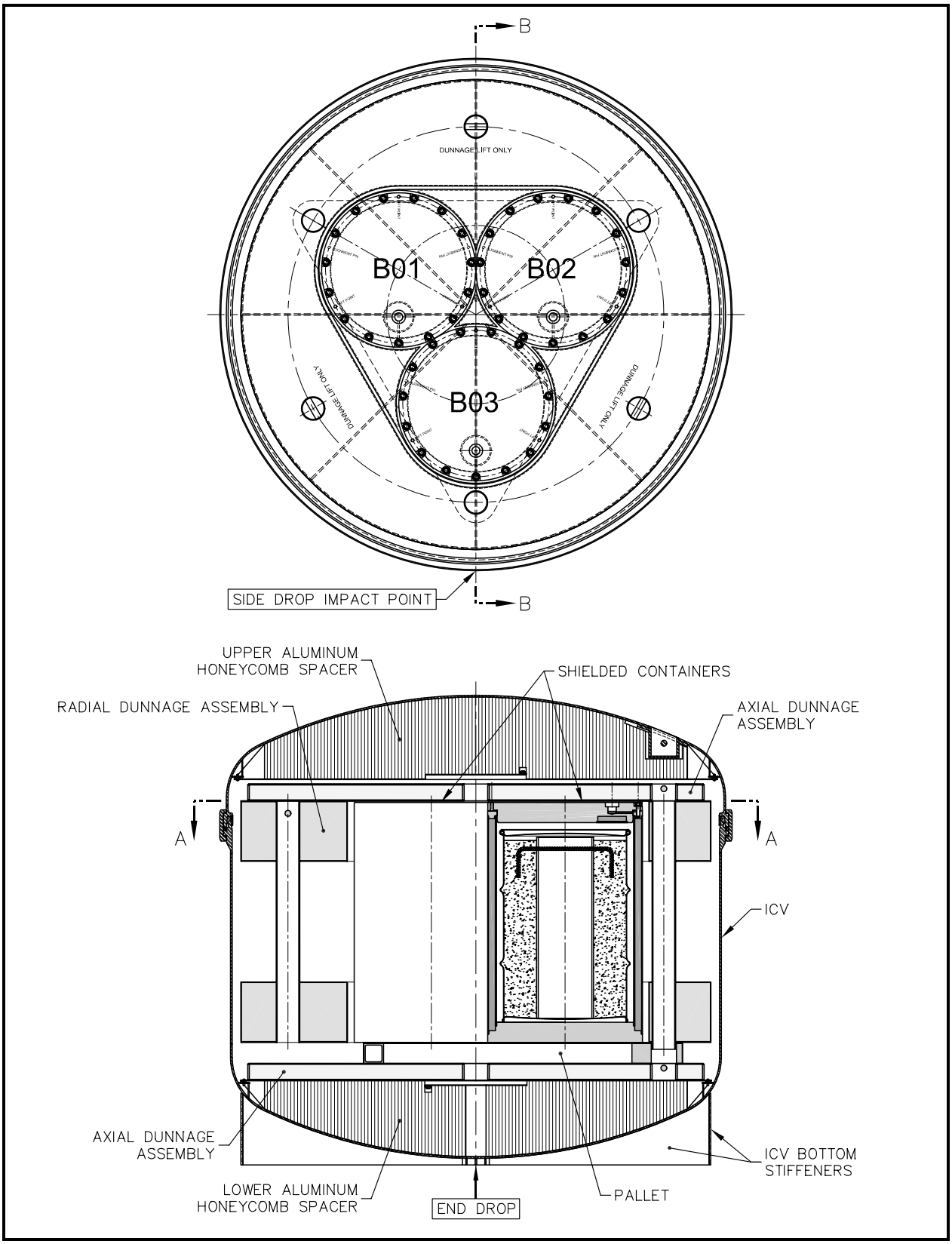

Figure 7 – Test Configuration and Orientations

For the ambient temperature (70 ºF) side drop, a 4⅝-inch radial crush was observed for the radial dunnage assembly. Unlike for the case of end drop where axial dunnage foam strength and its sensitivity to temperature have been shown to be of little importance, for side drop the strength and temperature sensitivity of the radial dunnage foam is a primary contributor to system response. Using an as-installed/as-tested, average room temperature, perpendicular-to-rise radial dunnage foam strength of 492.9 psi (the average of the two buns used to fabricate the radial dunnage: 475.6 psi for one bun, and 510.2 psi for the other bun) and the corresponding minimum allowed, room temperature strength of 430 psi (per note 15 of the shielded container SAR drawing), the impact of temperature variations on maximum deformation of the radial dunnage assembly and on the structural response of the shielded containers is addressed in Section 5.2, *Temperature*, below. Other data used in that section includes the observed crush of the HalfPACT OCA (3¾ inches) in a 30-foot side drop (see Table 2.10.3-3 of the HalfPACT SAR [3]).

5.2 Temperature

As indicated above and in Section 6.2, *Free Drop Tests*, below, the end and side drop tests were performed at the prevailing ambient temperatures of 77 ºF and 70 ºF, respectively. The significance of cold (-20 ºF) and hot (160 ºF bounding maximum for all payload components of interest) temperature extremes are addressed as follows.

5.2.1 Cold

5.2.1.1 End Drop

As established in Section 5.1.1, *End Drop*, for an end (axially oriented) drop, the aluminum honeycomb spacer material is the crushable medium of interest. Considering that crush of the aluminum honeycomb material is a buckling defined process, and that buckling is directly proportional to the material's elastic modulus and/or yield strength, the expected increase in acceleration at cold (-20 ºF) conditions versus ambient conditions is no more than 5% considering a wide range of aluminum grades (see Figures 3.2.1.1.1(d), 3.2.1.1.4, 3.2.3.1.4, 3.5.1.1.4 and 3.6.2.2.1(b) of MIL-HDBK-5J [6]). With steel and lead yield strengths exhibiting similar, if not slightly greater, strength increases over this same temperature range (e.g., see Table 2.3-2 of the RH-TRU 72-B SAR [5] for representative lead properties), the cold drop response of the shielded containers will not be substantially different than the ambient temperature drop response.

Therefore, based on a room temperature axial acceleration of 59.1*g* from Section 5.1.1, *End Drop*, the maximum cold case acceleration would remain relatively modest at $1.05 \times 59.1g = 62.1g$, with the slight increase in acceleration readily offset by the corresponding increases in shielded container lead and steel strengths.

5.2.1.2 Side Drop

From Section 5.1.2, *Side Drop*, the radial dunnage compressed approximately 4⅝ inches for an ambient condition side drop. A similar, but somewhat smaller OCA crush distance of 3¾ inches was observed for the side drop testing of a HalfPACT package. As such, for the specific side drop orientation of the radial dunnage that was tested, the shielded containers would experience lesser impact decelerations than would the overall HalfPACT package system.

However, to be conservative, it can be assumed that the maximum side drop deceleration that can ever be imposed on a shielded container corresponds to the maximum possible HalfPACT package system deceleration resulting from the 3¾ inch side crush. Given the cylindrical geometry of the HalfPACT OCA, its force-deflection relationship can be bounded on the low end by an assumed constant force resistance, and on the high end by an assumed linearly varying force-deflection relationship. Given these two extremes, a bounding impact deceleration can be established as follows.

For a constant force resistance, $E = W(h + \delta) = F\delta = WG\delta$, or equivalently, $G = (h + \delta)/\delta$, where W is the system weight (lb), F is the force magnitude (lb), the drop height, h = 360 inches, the maximum deflection, $\delta = 3.75$ inches, and the lower-bound impact acceleration, G, is:

$$G = \frac{h+\delta}{\delta} = \frac{360+3.75}{3.75} = 97g$$

For a linearly increasing force resistance, $E = W(h + \delta) = (F_{max}/2)\delta = (WG_{max}/2)\delta$, or equivalently, $G_{max} = 2(h + \delta)/\delta$, where W is the system weight (lb), F_{max} is the peak force reached at the maximum deflection, $\delta = 3.75$ inches, and the upper bound impact acceleration, G_{max}, is:

$$G_{max} = \frac{2(h+\delta)}{\delta} = \frac{2(360+3.75)}{3.75} = 194g$$

Assuming each shielded container is a simply supported beam that ignores the stiffening effects of the lead between the inner and outer shells, the unit stress in the shells due to bending, σ, is:

$$\sigma = \frac{Mc}{I} = \frac{(10{,}097)(11.49)}{1{,}170} = 99.2\ \text{psi}/g$$

where the maximum bending moment, very conservatively assuming a uniformly distributed load, $M = wL^2/8 = (63.2)(35.75)^2/8 = 10{,}097$ in-lb, the uniform load, w = W/L = 63.2 lb/in, the total weight, W = 2,260 pounds, the length, L = 35.75 inches, and the distance to the outer surface, c = 11.49 inches (the outer shell outer diameter is determined in the next paragraph).

From HalfPACT SAR drawing 163-008 [3], using the inner shell inside diameter, $D_i = 20.35$ inches, and for 7-gauge inner shell material ($t_i = 0.1793$ inches thick), and using the outer shell inside diameter, $D_o = 22.74$ inches, and for 11-gauge outer shell material ($t_o = 0.1196$ inches thick), the total composite moment of inertia of the inner and outer shells is:

$$I = \frac{\pi}{64}\left\{\left[(D_i + 2t_i)^4 - D_i^4\right] + \left[(D_o + 2t_o)^4 - D_o^4\right]\right\} = 1{,}170\ \text{in}^4$$

Using the maximum estimated side drop acceleration of 194*g*, the corresponding maximum stress in the outer shell, $\sigma_{max} = \sigma G_{max} = (99.2\ \text{psi}/g)(194g) = 19{,}245$ psi. Given the ASTM A1011, Grade 45, carbon steel shell's minimum room temperature yield strength of 45,000 psi, and given the conservatism of the above analysis, it is readily concluded that the shielded containers will withstand a cold side drop with no significant deformations occurring to the shielded container structure.

5.2.2 Hot

5.2.2.1 End Drop

Considering the same MIL-HDBK-5J [6] figures referenced in Section 5.2.1.1, *End Drop*, the decrease in aluminum honeycomb strength for a temperature change from 70 ºF to 160 ºF is again very limited. From those figures, a 5% change is appropriate. As such, in a hot condition end drop, the 6.2-inch stroke of the shielded containers relative to the ICV dished head, as measured for the ambient condition drop, can be increased to 1.05 × 6.2 = 6.51 inches. This represents a bounding hot condition crush distance that can be utilized in the HAC shielding evaluation.

Relative to impact accelerations, the 5% decrease in aluminum honeycomb strength at hot versus ambient temperatures can be expected to reduce ambient temperature impacts by 5% from 59.1*g* to 56.3*g*. However, since lead strength will reduce by more than 5% for a temperature increase from 70 ºF to 160 ºF, it is necessary to address the response of the lead in a hot end drop. This can be conservatively done by assuming the surrounding steel shells will not provide any support to the lead column and, therefore, that the lead column must support its own inertia. From 30-foot free drop testing and associated post-drop shielding integrity testing and confirmatory sectioning of one of the shielded containers, ambient temperature drop testing has been shown to result in no significant lead slump. The following calculation demonstrates that the lack of lead slump observed for ambient temperature drop conditions is physically reasonable, and that the increase in slump in going from ambient to hot (160 ºF) conditions is a maximum of 0.079 – 0.056 = 0.023 inches. This minor additional slump, which occurs outboard of the ends of the shielded container payload cavity, is of no significance to the shielding performance of the container.

With reference to Figure 2.3-6 of the RH-TRU 72-B SAR [5], at the end drop test temperature of 77 ºF and at hot (160 ºF) conditions, the corresponding compressive stress strain curves for lead can be approximated as follows:

Strain (%)	Stress (psi) at Temperature	
	77 ºF	160 ºF
0.0	300	200
0.3	—	500
0.5	700	—
1.0	900	750

With a lead column height, h, of 31.375 inches and a lead density, ρ, of 0.41 lb/in^3, the stress, σ, in the lead under an applied acceleration, G, will vary linearly along the length of the lead column and at any location, x (with x being 0.0 at the top of the column), becomes:

$$\sigma = \rho G x$$

The resultant stress and strain in the lead versus lead column position, x, becomes as follows for an ambient acceleration, G_a, of 59.1*g* and a hot acceleration G_h, of 56.3*g*.

Lead position, x (inches, from top of column)	59.1*g* at 77 ºF		56.3*g* at 160 ºF	
	Stress (psi)	Strain (%)	Stress (psi)	Strain (%)
0.000	0	0.000	0	0.000
8.664			200	0.000
12.381	300	0.000		
21.661			500	0.300
28.889	700	0.500		
31.375	760	0.650	724	0.927

The resultant shortening (or slump) of the lead column for the ambient condition case becomes:

$$\Delta L = (28.889 - 12.381)(0.00500)/2 + (31.375 - 28.889)(0.00650 + 0.00500)/2 = 0.056 \text{ inches}$$

The resultant shortening (or slump) of the lead column for the hot condition case becomes:

$$\Delta L = (21.661 - 8.664)(0.00300)/2 + (31.375 - 21.661)(0.00927 + 0.00300)/2 = 0.079 \text{ inches}$$

5.2.2.2 Side Drop

For the hot side drop case, the bounding deceleration established for side drop in Section 5.2.1.2, *Side Drop*, of 194*g* can again be conservatively employed. At 194*g*, from Section 5.2.1.2, *Side Drop*, the side drop induced stress in the shielded container outer shell is 194 × 99.2 = 19,245 psi, which remains well below the yield strength of the A1011, Grade 45, shell at 160 ºF.

To conservatively bound the maximum crush of the radial dunnage assembly at hot conditions, the observed ambient condition crush of 4⅝ inches must first be multiplied by a factor of 1.333, to account for the reduction in foam strength when going from 70 °F to 160 °F. Per Section 2.10.3.5.1.2 of the TRUPACT-II SAR [4], foam strength reduces to approximately 75% of its room temperature strength for this temperature change. With crush volume being inversely proportional to foam crush strength, the crush volume at hot conditions becomes 1/0.75 = 1.333 times the ambient temperature crush volume. An additional factor is needed to address the fact that the minimum room temperature foam strength is 430 psi versus the as-installed/as-tested foam strength of 492.9 psi (see Section 5.1.2, *Side Drop*). Again, using an inversely proportional relationship, the adjustment factor becomes 492.9/430 = 1.146. The extrapolated crush of the radial dunnage to hot conditions therefore becomes 4⅝ × 1.333 × 1.146 = 7.07 inches. With an initial foam thickness calculated from the shielded container SAR drawing of 9.08 inches, approximately 2 inches of uncrushed foam would still remain, which corresponds to a maximum foam strain of 77.9% (i.e., 7.07/9.08 = 0.779). This represents a bounding hot condition radial dunnage strain and a corresponding crush distance that can be utilized in the HAC shielding evaluation.

5.3 Pressure

Except for investigating the potential for any adverse payload to ICV interactions, the 30-foot free drop tests were not intended to address ICV performance, hence, it was not necessary to include internal pressure within the ICV. In fact, the ICV used for testing did not include a locking ring and was assembled without O-ring seals, thus making pressurization impossible. The effect of a 50 psig external pressure on the foam filled dunnage assemblies and lead backed shielded container outer shell assemblies is also of little significance and did not warrant testing within a pressurized ICV.

6.0 TEST RESULTS

6.1 Component Weights

With the exception noted in Section 6.2.3, *Horizontal Side Drop Test Preparation and Test*, component weights are summarized in Table 1. Testing with a 560-pound payload container within each shielded container was conservative and resulted in a total gross weight of each loaded shielded container that exceeded its 2,260-pound weight limit. Additionally, the gross weight of all payload assembly components was equal to the maximum authorized content weight limit for the HalfPACT package.

Table 1 – Component Weights (lb)

Component	Subassembly Weight	Assembly Weight
ICV Lid	603	
ICV Body	1,359	
Upper Spacer	88	
Lower Spacer①	78	
ICV Assembly		*2,128*
Shielded Container 1	1,705	
Payload Drum 1	560	
Shielded Container 2	1,711	
Payload Drum 2	560	
Shielded Container 3	1,710	
Payload Drum 3	560	
Triangular Spaceframe Pallet	110	
Radial Dunnage	428	
Upper Axial Dunnage	128	
Lower Axial Dunnage①	128	
Payload Assembly		*7,600*
Total Tested Weight		**9,728**

Notes:

① The lower aluminum honeycomb spacer and lower axial dunnage (206 pounds, total) were replaced by a temporary lower spacer structure (158 pounds) for the side drop; see Section 6.2.3, *Horizontal Side Drop Test Preparation and Test*.

6.2 Free Drop Tests

Based on the justification provided in Section 5.1, *Justification for Testing Only End and Side Orientations*, two 30-foot free drop tests were performed: 1) a vertical end drop and, 2) a horizontal side drop.

Fluorescein dye powder was mixed with dry flour and placed within each shielded container as a means for determining whether confinement integrity was compromised (see Figure 8, Figure 9, Figure 10, and Figure 11). Fluorescein dye, when activated by water, fluoresces yellow-green in both the ultraviolet and visible light spectrum.

Figure 8 – Installing and Cutting the Fluorescein Dye Bags

Figure 9 – Wetting the Container to Activate the Fluorescein Dye

Figure 10 – Fluorescein Dye within the Shielded Container Body

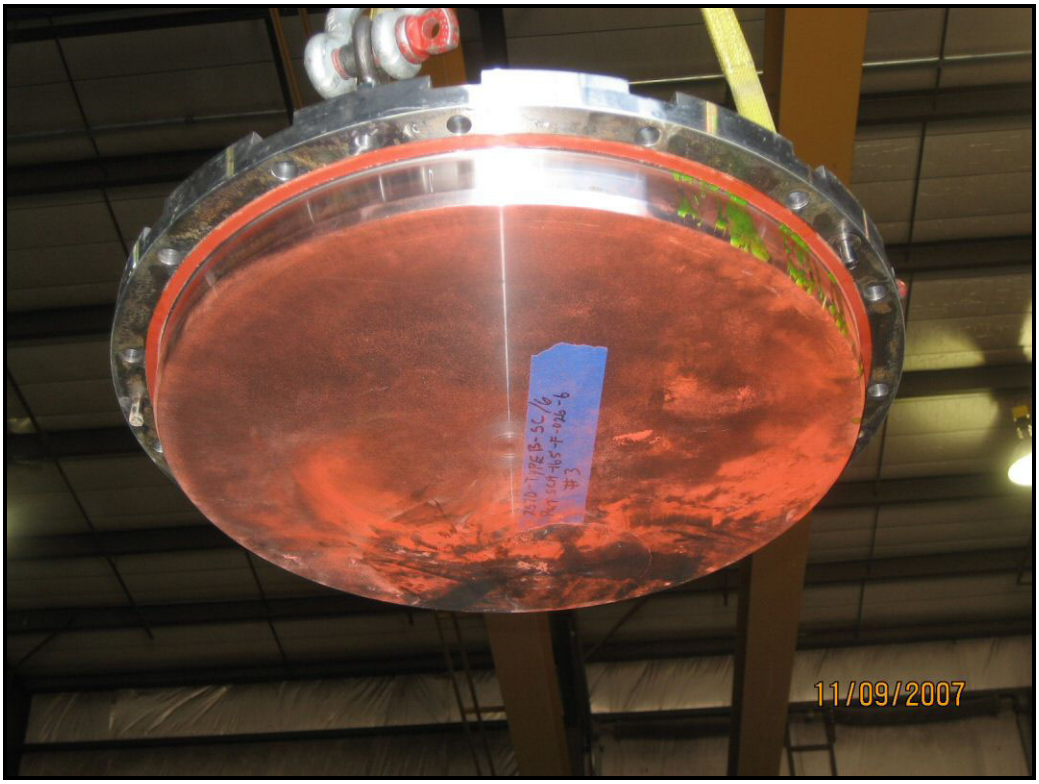

Figure 11 – Fluorescein Dye under the Shielded Container Lid

Shielding integrity tests were performed before and after the free drop tests on each shielded container to determine whether shielded integrity was compromised. Discussion of shielding integrity testing is provided in Section 6.3, *Shielding Integrity Testing*.

6.2.1 Vertical End Drop Preparation and Test

The following list summarizes the end drop test parameters:

- tightened all shielded container lid closure screws to 85 ±10 lb-ft torque at final assembly
- installed test shielded containers 1 and 3 in a normal transport orientation (i.e., lids oriented upward), and test shielded container 2 in an inverted orientation (i.e., lid oriented downward) (see Figure 5 and Figure 16)
- verified the vertical angle as 0º ±2º (see Figure 12; maximum actual angle 1º from vertical)
- verified the free drop height as 30 feet, +3/-0 inches
- measured the temperature to be 77 ºF at the time of the drop test
- conducted the drop test at 4:30 p.m. on Thursday, 11/08/2007 (see Figure 13)
- witnessed a small rebound of approximately 5 inches during the impact event
- observed visible deformation to the ICV assembly near the bottom (see Figure 14 and Figure 15)

6.2.2 Post-End Drop Test Disassembly

The following list summarizes the end drop results:

- measured the pre-test axial height of 52.79 inches from the inside bottom of the ICV body to the top of the shielded containers (see Figure 16 for the relative position of components)
- measured the post-test axial height of 46.59 inches from the inside bottom of the ICV body to the top of the shielded containers (see Figure 17 for the relative position of components)
- calculated axial deformation of the payload components of 52.79 – 46.59 = 6.20 inches
- measured axial deformation of the ICV body of 1/8 inch
- observed significant damage to the lower axial dunnage, and lower aluminum honeycomb spacer (see Figure 18, Figure 20, Figure 21, and Figure 19) indicating that the majority of the payload's kinetic energy went into deforming these components; the triangular spaceframe pallet had little damage consisting mostly of minor weld cracks
- observed no significant deformation of, or damage to, the shielded containers
- observed no significant deformation of, or damage to, the ICV attributable to interaction with the payload

Figure 12 – 30-foot End Drop

Figure 13 – Instant of End Drop Impact

Figure 14 – End Drop Hoop Damage to the ICV Shell (Overall)

Figure 15 – End Drop Hoop Damage to the ICV Shell (Close-Up)

Figure 16 – Pre-End Drop Relative Position of Components

Figure 17 – Post-End Drop Relative Position of Components

Figure 18 – Deformed Pallet, Axial Dunnage, and Lower Spacer

Figure 19 – Deformed Lower Axial Dunnage from End Drop

Figure 20 – Deformed Lower Spacer (from End Drop; Top View)

Figure 21 – Deformed Lower Spacer (from End Drop; Bottom View)

6.2.3 Horizontal Side Drop Test Preparation and Test

The following list summarizes the side drop test parameters:

- fabricated and installed a triangular-shaped lower spacer structure to replace the irreparable and unusable lower axial dunnage and lower honeycomb spacer (see Figure 22); this temporary lower spacer structure was designed to position the remaining payload components and shielded containers in their correct axial location prior to the side drop test, and to not interfere with the side drop test; weighing 158 pounds, the temporary structure was 48 pounds less than the 206-pound combined weight of the lower axial dunnage and lower aluminum honeycomb spacer
- installed all test shielded containers in the normal transport orientation (i.e., lids oriented upward) without the plastic stretch wrap (see Figure 23)
- oriented test shielded container 3 to be at the lowest position (see Figure 23); this orientation conservatively placed the least thickness of radial dunnage foam in the plane of impact
- verified the horizontal angle as 0º ±2º (see Figure 24; actual angle 2º from horizontal, but configured to simultaneously contact the seal flange tabs and lower torispherical head knuckle)
- verified the free drop height as 30 feet, +3/-0 inches
- measured the temperature to be 70 ºF at the time of the drop test
- conducted the drop test at 10:14 a.m. on Friday, 11/09/2007 (see Figure 25)
- witnessed a small rebound of approximately 9 inches during the impact event (see Figure 26)
- measured approximately 26-inch wide flattening along the ICV's length, corresponding to an external crush depth of approximately 2¼ inches; in comparison, from the HalfPACT SAR for CTU Test 2 [3], the measured permanent deformation were flats 37 inches wide at the OCA top and bottom, corresponding to a crush depth of approximately 3¾ inches (see Figure 27)

6.2.4 Post-Side Drop Test Disassembly

The following list summarizes the side drop results:

- measured the pre-test radial dunnage thickness of 9⅜ inches through the impact plane (see Figure 23 for the relative position of components)
- measured the post-test radial dunnage thickness of 4¾ inches through the impact plane (see Figure 28 and Figure 29 for the relative position of components)
- calculated radial deformation of the radial dunnage of 9⅜ – 4¾ = 4⅝ inches
- observed virtually identical performance between the upper and lower portions of the radial dunnage, even though several glued foam-to-foam interfaces, which were purposely oriented and aligned differently at each end, did exist; this demonstrated the lack of significance to the use of glued foam-to-foam interfaces and where they are located
- observed very modest damage to the upper axial dunnage assembly and upper aluminum honeycomb spacer, and significant localized damage to the radial dunnage (see Figure 30 and

Figure 31) indicating that the vast majority of the payload's kinetic energy went into deforming this component

- observed no significant deformation of or damage to the shielded containers (see Figure 32 and Figure 33) ; exterior damage was limited to localized crushing of the upper and lower outer shell welds (circumferential) at the contact points between shielded containers, and interior deformation at the 30-gallon drum rolling hoop interfaces was of no significance; the filter port lead shield plug cover plates and adjoining welds showed no signs of permanent deformation on any of the shielded containers
- observed no significant deformation of, or damage to, the ICV attributable to interaction with the payload
- observed no fluorescein dye on the exterior of all three shielded containers indicating that confinement integrity was maintained (see Figure 9, Figure 32, and Figure 33)
- shielding integrity testing indicated no significant change in shielding capabilities of the design (see Section 6.3, *Shielding Integrity Testing*)

Figure 22 – Temporary Lower Spacer Structure Used for Side Drop

Figure 23 – Pre-Side Drop Test Shield Container Configuration

Figure 24 – Side Drop Impact Orientation (2º Off True Horizontal)

Figure 25 – 30-foot Side Drop

Figure 26 – Instant of Side Drop Impact/Rebound

Figure 27 – Deformed ICV Lid (~26” Flat) after Side Drop

Figure 28 – Lateral Shifting of the Payload after Side Drop

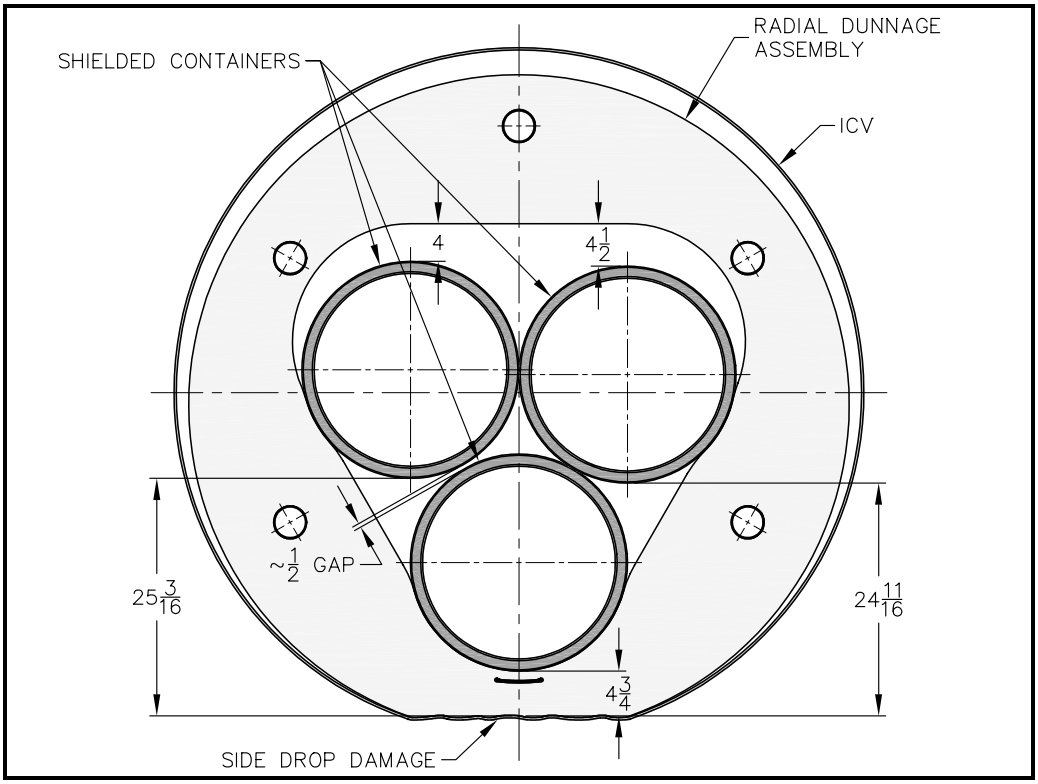

Figure 29 – Dimensions Relating the Shifted Shielded Containers

Figure 30 – Side Drop Deformed Radial Dunnage (Outside View)

Figure 31 – Side Drop Deformed Radial Dunnage (Inside View)

Figure 32 – Negligible Visible End or Side Drop Damage

Figure 33 – Side Drop Damage Limited to Localized Weld Crushing

6.3 Shielding Integrity Testing

Pre- and post-drop shielding integrity testing involved the use of a Ludlum 44-10 sodium-iodide, two-inch diameter scintillator detector inside a collimator, a Ludlum 2530-1 logging survey meter interfaced with a laptop computer, and a 10 micro-curie Cobalt-60 source.

A tripod apparatus was mounted to the shielded container's bolting flange and used to control the detector/source spacing and location. The source was attached to a bar on the center axle and the detector/collimator to an outer cantilevered arm (see Figure 34).

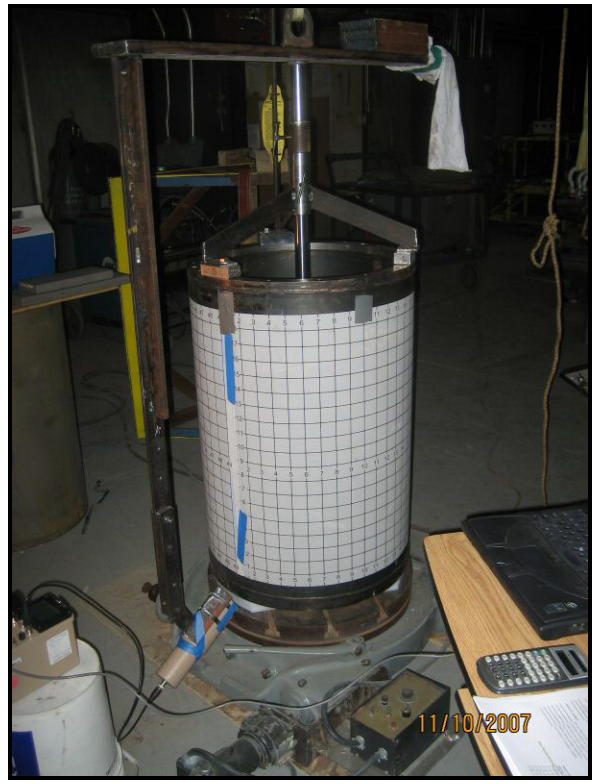

Figure 34 – Scanning Apparatus

A gridded Mylar overlay facilitated measurement repeatability at the defined grid locations. The zero circumferential position was arbitrarily set at the outer shell's longitudinal seam weld and the zero axial position was set at the elevation of the inner surface of the base. Each axial row consisted of 49 sets of circumferential readings, with 24 total axial rows. The lowest axial reading (-2 position) was centered on the outer shell-to-base circumferential weld seam at an elevation 1½ inch below the inner surface of the base and 1/2 inch below the lead-to-base interface. The next lowest axial reading (-1 position) was located 3/4 inch above at an elevation 3/4 inch below the inner surface of the base and 1/4 inch above the lead-to-base interface. The highest axial reading (21 position) was located 3/8 inch above the lead-to-flange interface, and the next-to-highest axial reading (20 position) was located 3/8 inch below the lead-to-flange interface. The remaining axial elevation positions maintained a 1½ inch grid spacing with the circumferential grid spacing being equal.

Due to the source being located as close as possible to the inner surface of the base for readings at axial positions -1, -2, and 0, the source-to-detector distance and corresponding angular orientation of the detector deviated from the other straight-line source-to-detector alignment and constant distance setup. Due to geometry constraints, the -2, -1, 0, 20, and 21 axial positions measured material attenuation that deviated from the other scans that were exclusively measuring the attenuation provided by the inner and outer steel shells and the interstitial lead at full thickness. Figure 35 illustrates the circumferential and axial grid maps.

The purpose of the shielding integrity testing was to evaluate any potential reduction in shielding effectiveness of the steel and lead composite body shield as a result of the HAC drop tests. A shielding effectiveness change map was generated for each of the units by calculating the percent difference in measured dose rate at each grid location for the pre- and post-drop readings with a 10% change threshold selected to prompt further evaluation. Figure 36, Figure 37, and Figure 38 illustrate the pre-and post-drop test percent difference in measured dose rate for shielded container test units B01, B02 (inverted in end drop), and B03 (lowermost in side drop), respectively.

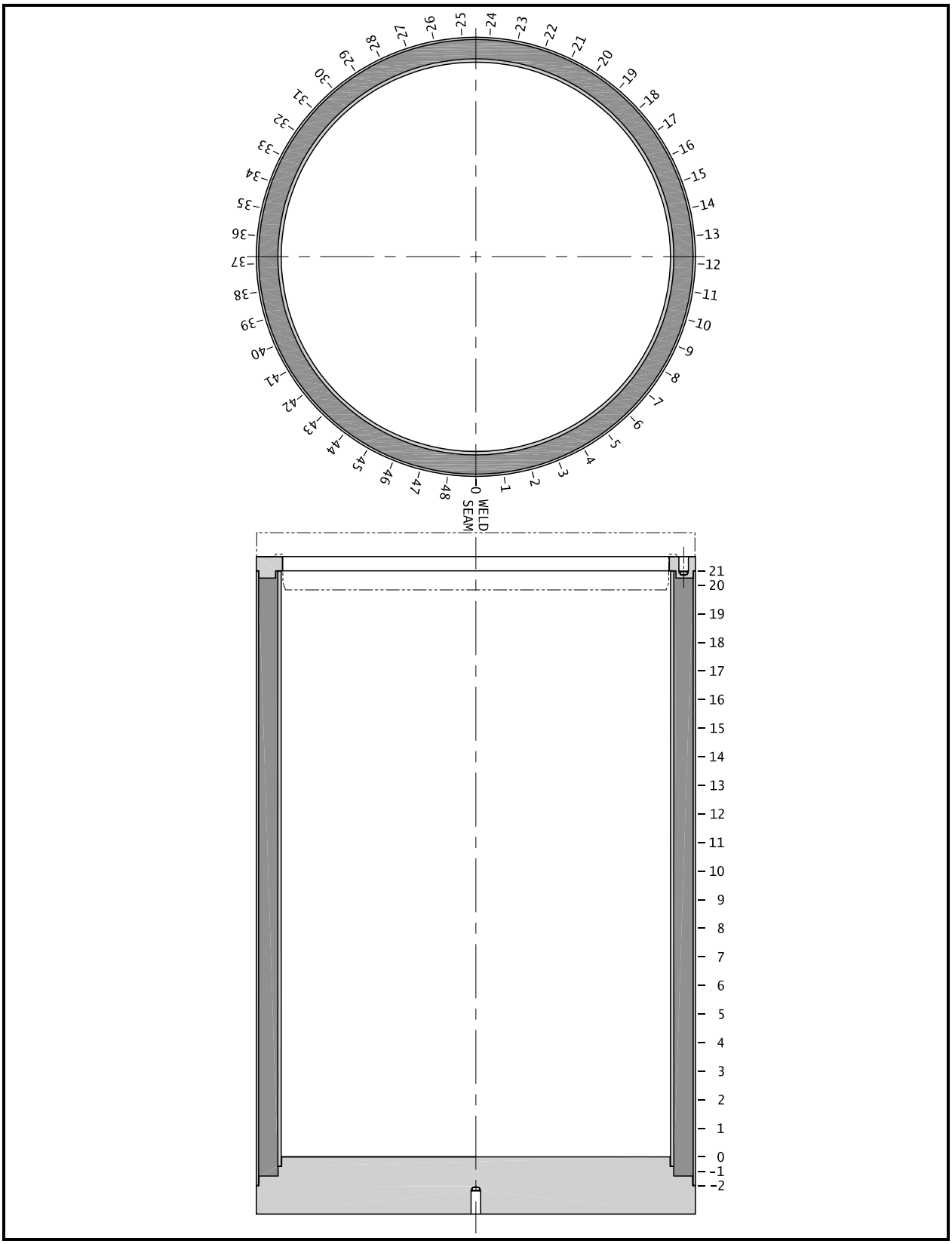

Figure 35 – Circumferential and Axial Scan Grid Map

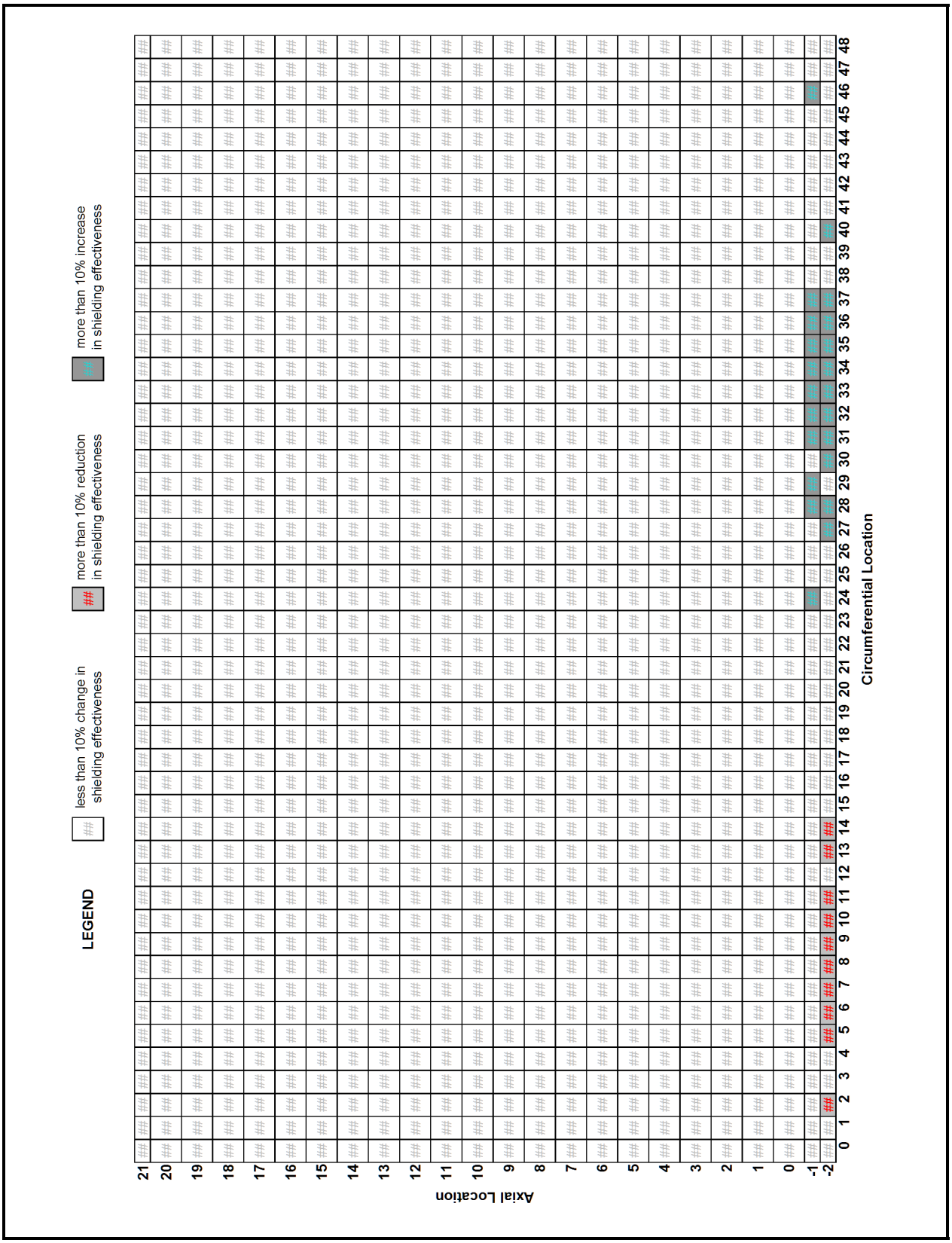

Figure 36 – Shielding Change on Test Shielded Container B01

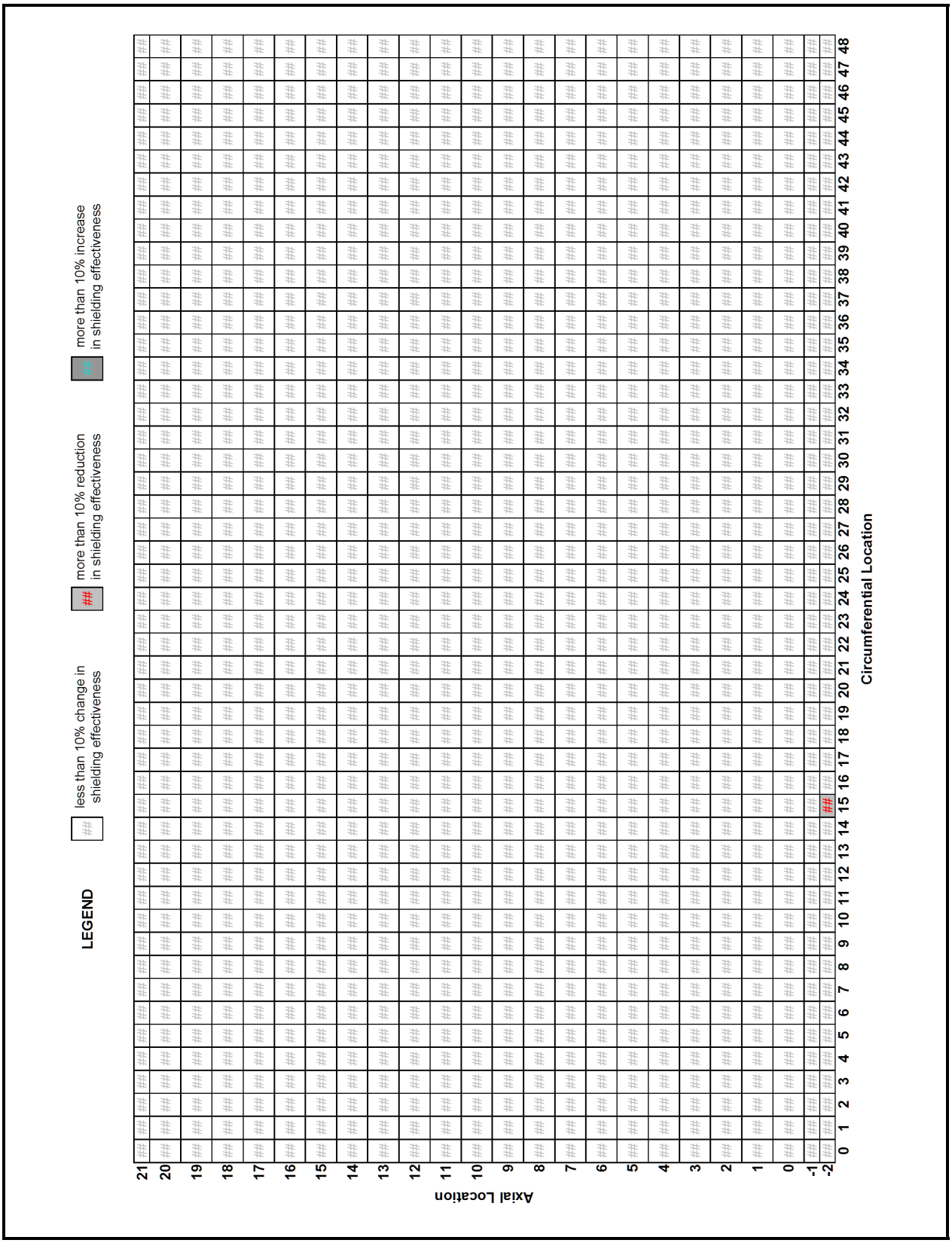

Figure 37 – Shielding Change on Test Shielded Container B02

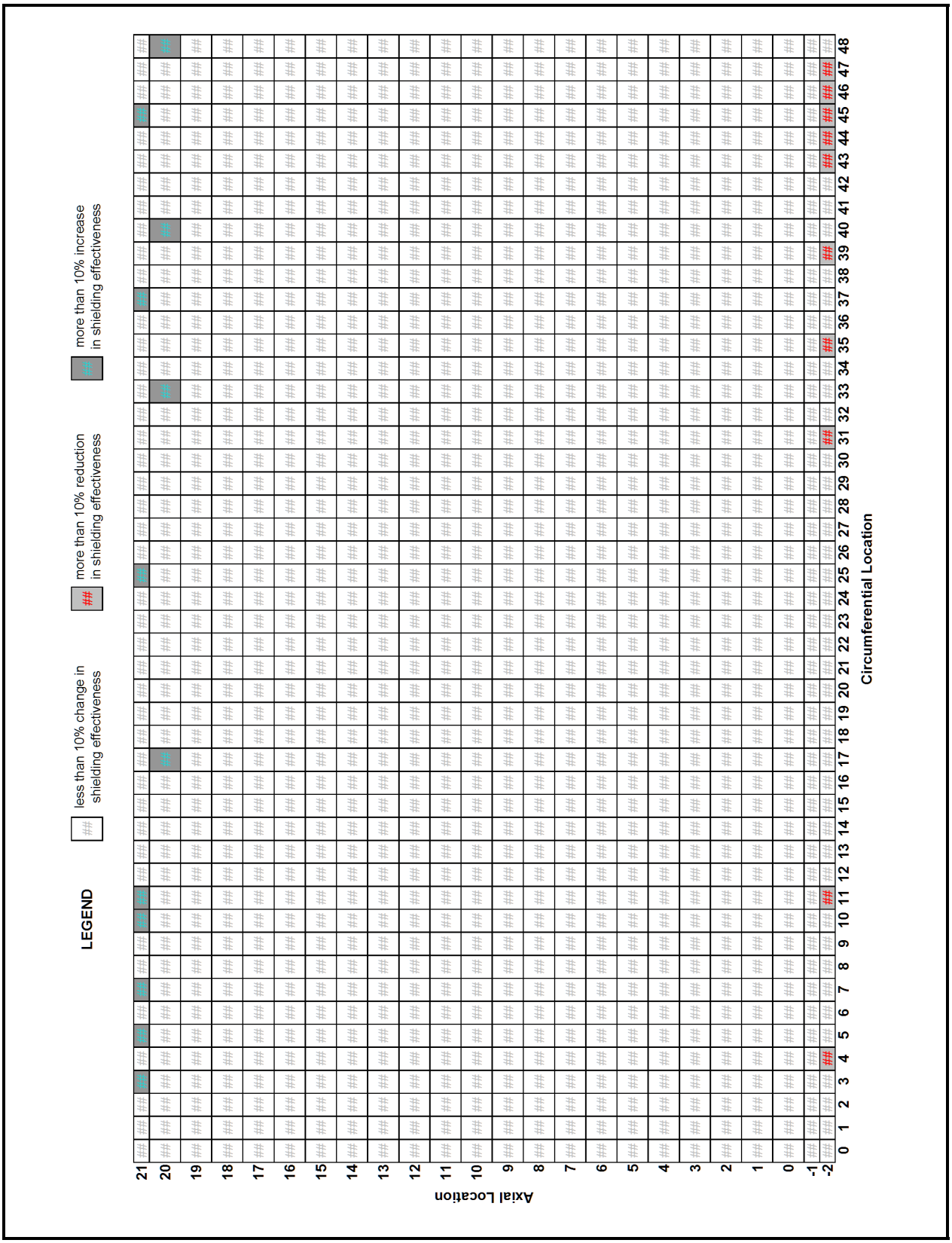

Figure 38 – Shielding Change on Test Shielded Container B03

As can be seen in Figure 36, Figure 37, and Figure 38, select locations at the lower axial and upper axial elevations show a percent difference that exceeds either a 10% increase or reduction in shielding effectiveness, with all remaining grid locations indicating no appreciable change as a result of the drop events. At all grid locations for all three test units, the percent difference in pre- and post-drop dose rate readings did not exceed 20%. Because the -1 and -2 axial elevations are below the inner surface of the base and the data is subject to additional measurement variation due to a) the non-straight-line alignment of the source and detector and b) the angular offset of the source and detector resulting in measurements through a slice-section of the thick steel base, the greater than 10% change in these locations is not considered representative of a decrease (or increase) in shielding effectiveness at these locations based on the process parameters described above. Because the 20 and 21 axial elevations are above the inner surface of the lid and the data is subject to additional measurement variation due to streaming effects out of the container in the tested (lid removed) configuration, the greater than 10% change in these locations is also not considered representative of a decrease (or increase) in shielding effectiveness at these locations based on the process parameters described above. Therefore, the shielding integrity testing indicates no significant change in the shielding occurred as a result of the HAC drop testing.

To supplement the shield integrity testing and validate the above conclusions, cross-sections (wall cut-outs) were taken from test shielded container B03, since it was the container subjected to the most cumulative damage. Two longitudinal sections were taken from unit B03, one at the side drop bottom dead center position (see Figure 39 and Figure 40) and one at the point of contact between B03 and B02 (see Figure 41 and Figure 42); the arrows indicate the lead/steel interface (Figure 39 is cut through the lead pour port, and the arrow shows the interface with the bottom of the lead cavity). As can be seen in Figure 40 and Figure 42, lead slump did not occur.

Finally, Table 2 presents lead thickness measurements taken at several positions along the length of the two axial slices. As shown, post-test lead thicknesses everywhere exceeded the 0.85-inch thickness assumed in the HAC shielding analyses. Further, it is observed that a lower bound on observed post-test lead thicknesses between the shell ends can be established by assuming a linearly varying thickness between ends, which per Flag Note 20 of HalfPACT SAR drawing 163-008, cannot be less than 0.94 inches. With reference to Table 2, for the bottom dead center slice, thickness away from the ends is seen to somewhat exceed end thicknesses. For the slice taken at the B03/B02 interface, lead thickness is seen to vary nearly linearly with length from 65/64 at the top to 61/64 at the bottom (only location D is slightly thicker, by 1/64 inch, than the simple linear assumption would indicate). Given these and other considerations, it is concluded from a study of the gamma scan records and destructive disassembly measurements that the small variations in lead thickness observed along the length and at varying circumferential positions identified post-test most likely reflect the state of the lead at pre-test conditions as opposed to changes resulting from free drop testing. In any event, the observed variations in gamma scan readings taken at the ends of the shielded container before and after free drop are of no significance relative to the shielding capabilities of the design.

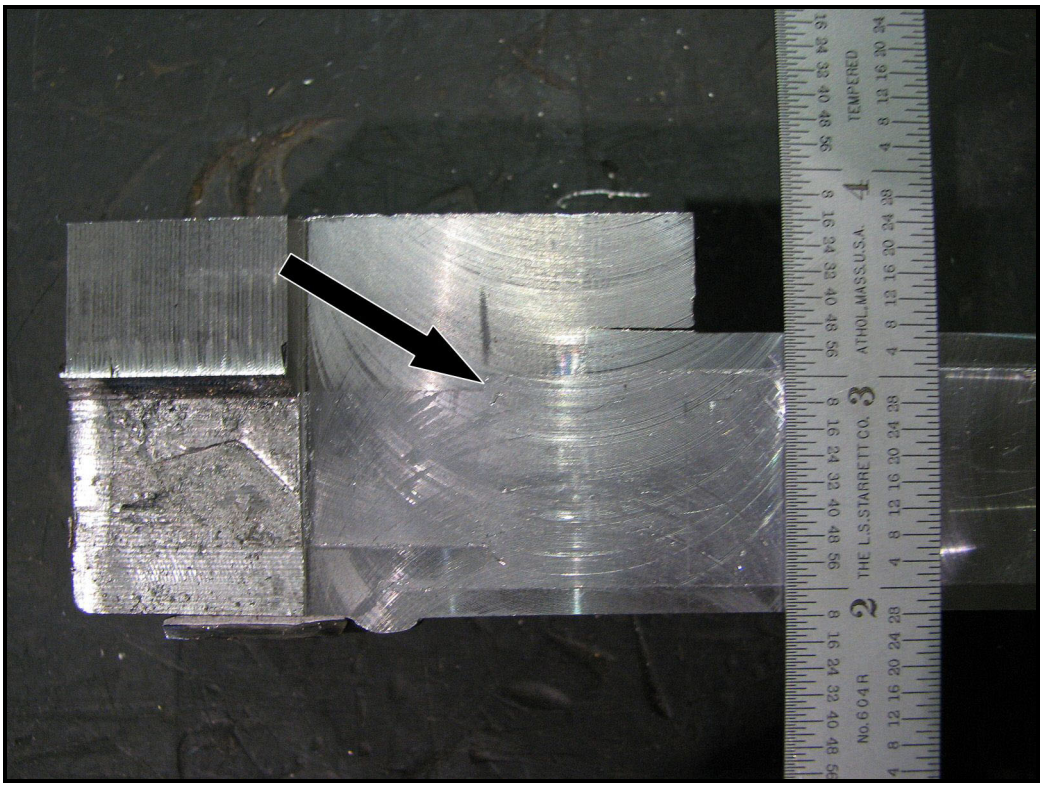

Figure 39 – Axial Slice in B03 at Lowest Point; Lower End

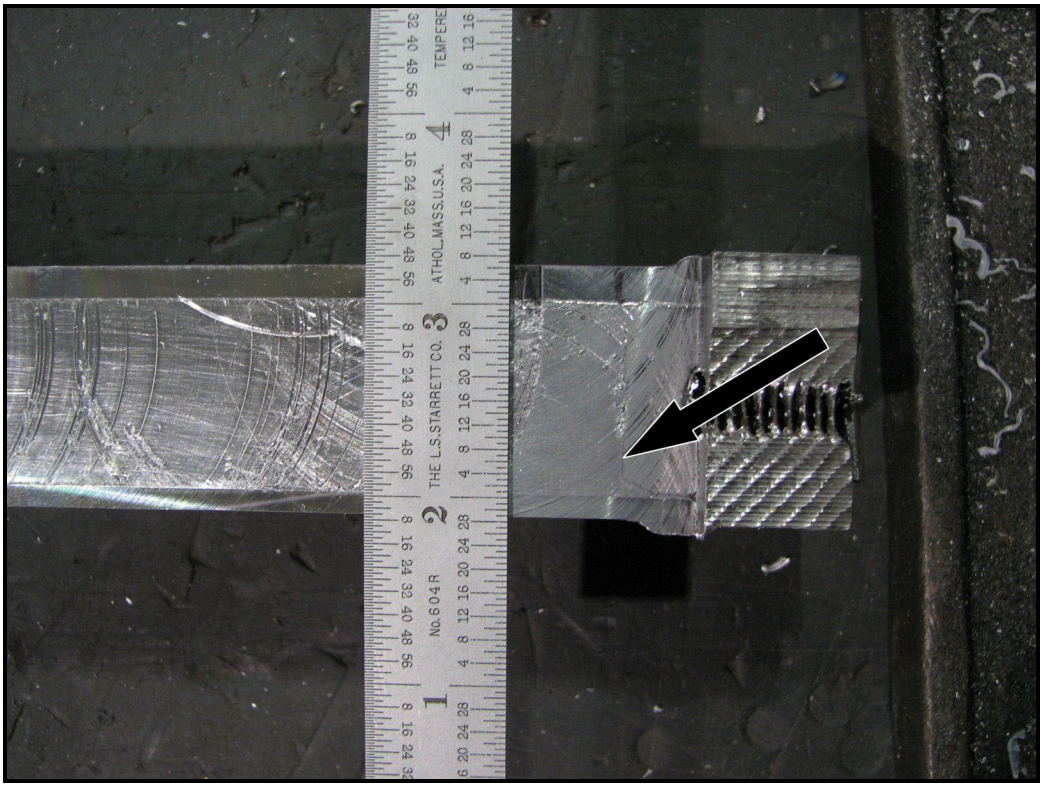

Figure 40 – Axial Slice in B03 at Lowest Point; Upper End

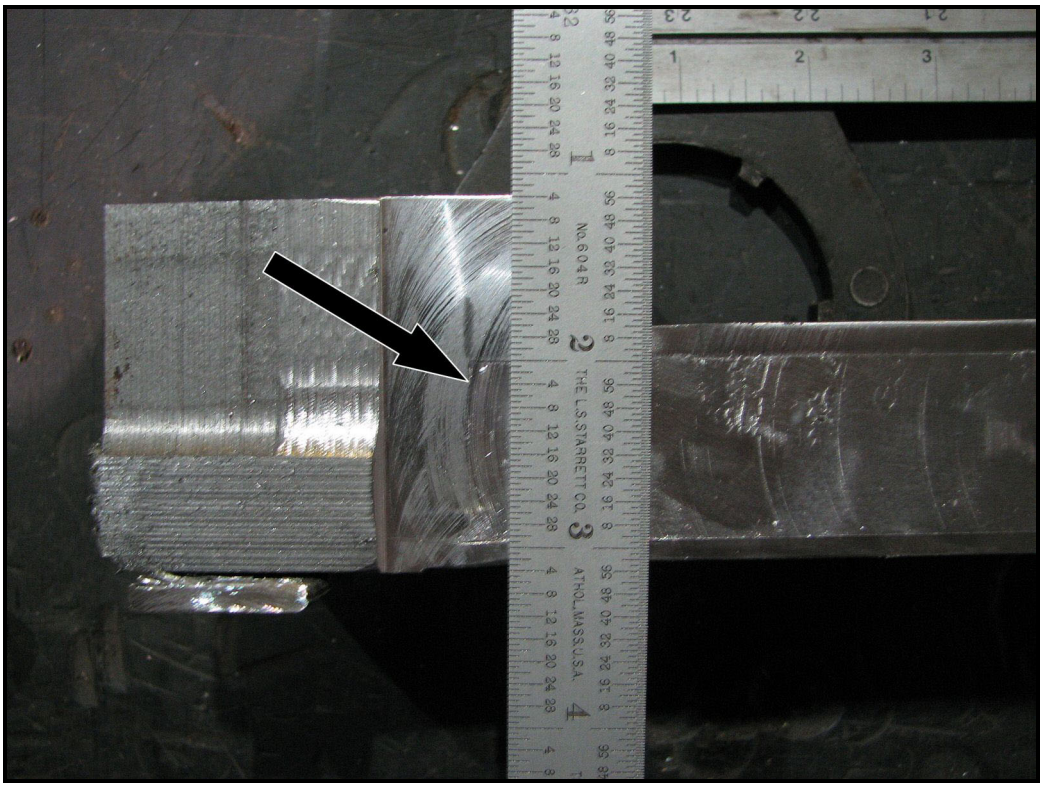

Figure 41 – Axial Slice in B03 at B02 Interface; Lower End

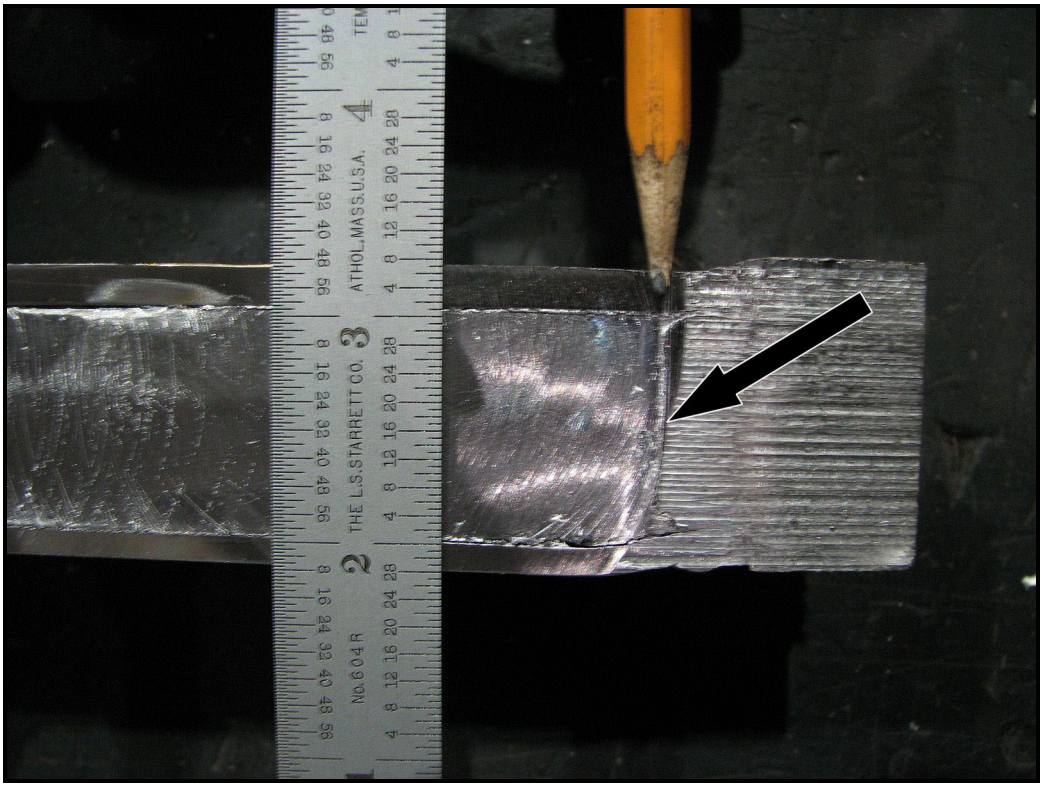

Figure 42 – Axial Slice in B03 at B02 Interface; Upper End

Table 2 – Measured Lead Thickness (Inches) in Test Unit B03 Axial Slices
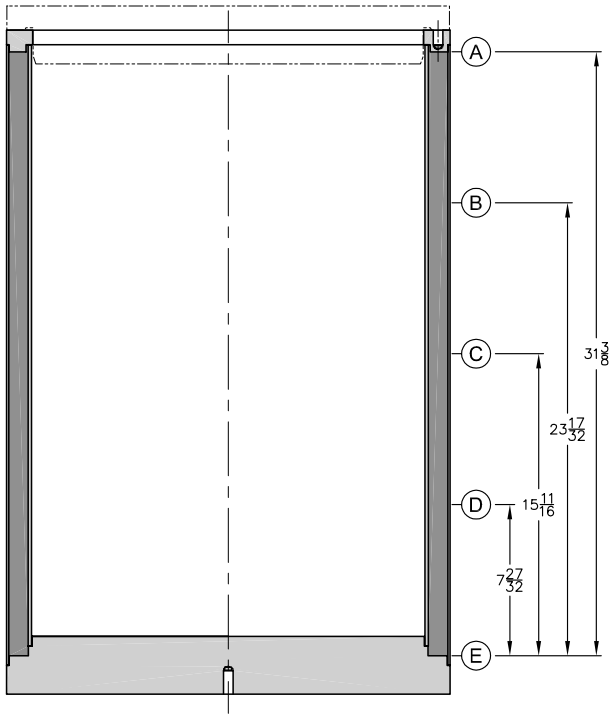
Interface with Dunnage (Bottom)	
Location	**Lead Thickness**
A	1
B	1-1/32
C	1-3/64
D	1-3/64
E	1
Average	1.025
Interface with Test Unit B02	
Location	**Lead Thickness**
A	1-1/64
B	1
C	63/64
D	63/64
E	61/64
Average	0.988